Membrane cholesterol as regulator of human rhomboid protease RHBDL4

Received for publication, February 26, 2018, and in revised form, August 18, 2018 Published, Papers in Press, August 24, 2018, DOI 10.1074/jbc.RA118.002640

Sandra Paschkowsky[‡], Sherilyn Junelle Recinto[‡1], Jason C. Young[§], Ana-Nicoleta Bondar[¶2], and Lisa Marie Munter[‡3]

From the [‡]Department of Pharmacology and Therapeutics and Cell Information Systems Group and [§]Department of Biochemistry and Groupe de Recherche Axé sur la Structure des Protéines, McGill University, Montreal, Quebec H3G 0B1, Canada and the [¶]Department of Physics, Theoretical Molecular Biophysics, Freie Universität Berlin, Arnimallee 14, Berlin 14195, Germany

Edited by Paul E. Fraser

In the last decade, intramembrane proteases have gained increasing attention because of their many links to various diseases. Nevertheless, our understanding as to how they function or how they are regulated is still limited, especially when it comes to human homologues. In this regard, here we sought to unravel mechanisms of regulation of the protease rhomboid-like protein-4 (RHBDL4), one of five active human serine intramembrane proteases. In view of our recent finding that human RHBDL4 efficiently cleaves the amyloid precursor protein (APP), a key protein in the pathology of Alzheimer's disease, we used established reagents to modulate the cellular cholesterol content and analyzed the effects of this modulation on RHBDL4-mediated processing of endogenous APP. We discovered that lowering membrane cholesterol levels increased the levels of RHBDL4-specific endogenous APP fragments, whereas high cholesterol levels had the opposite effect. Direct binding of cholesterol to APP did not mediate these modulating effects of cholesterol. Instead, using homology modeling, we identified two potential cholesterol-binding motifs in the transmembrane helices 3 and 6 of RHBDL4. Substitution of the essential tyrosine residues of the potential cholesterol-binding motifs to alanine increased the levels of endogenous APP C-terminal fragments, reflecting enhanced RHBDL4 activity. In summary, we provide evidence that the activity of RHBDL4 is regulated by cholesterol likely through a direct binding of cholesterol to the enzyme.

Rhomboid proteases are an ancient class of intramembrane proteases that received increasing interest in recent years (1). Multiple publications linked rhomboid functions to important cellular processes such as host invasion in toxoplasmodium (2, 3), innate immunity and regulation of inflammatory signaling (4), as well as mitochondrial homeostasis (5). In particular, there is evidence for the involvement of the mitochondrial rhomboid protease presenilin-associated rhomboid-like protein (PARL)[4] in Parkinson's disease and type II diabetes (6–8). In addition, our laboratory recently reported a potential link of the human rhomboid protease RHBDL4 to Alzheimer's disease (9).

Despite these interesting indications, there is only little information available on how mammalian rhomboid proteases function and how they are regulated (10). Human rhomboid proteases can be classified into proteolytically active (RHBDL1, RHBDL2, RHBDL3, RHBDL4, and PARL) and inactive pseudoenzymes that have lost the catalytically active residue during evolution (1). We recently found that members of the human amyloid precursor protein (APP) family are substrates of RHBDL4. The cleavage of APP through RHBDL4 is very efficient as full-length APP levels decrease by ~80%. Thereby, RHBDL4 generates distinct large APP C-terminal fragments that can be detected from endogenous APP upon RHBDL4 overexpression (9). Herein, we took advantage of this efficient RHBDL4–APP enzyme–substrate pair as it is ideal to study regulatory mechanisms of RHBDL4 by monitoring the production of endogenous RHBDL4-specific APP fragments.

It has previously been suggested that the membrane environment alters rhomboid protease activity (11, 12). Reconstitution of *Drosophila* Rho-4 and human RHBDL2 in different lipid environments alters not only the activity but also the specificity of the enzyme (13, 14). Furthermore, RHBDL4 was shown to locate to the endoplasmic reticulum (ER) (15, 16), a key organelle for lipid synthesis and cholesterol homeostasis. The ER membrane exhibits very low levels of membrane cholesterol (17) and is therefore destined to sense changes in cholesterol levels (18). Cholesterol homeostasis is predominantly achieved

This work was supported in part by Natural Sciences and Engineering Research Council of Canada (NSERC) Discovery Grant RGPIN-2015-04645 (to L. M. M.); Canada Foundation of Innovation Leaders Opportunity Fund CFI-LOF 32565; Alzheimer Society of Canada Young Investigator Award PT-58872 and Research Grant 17-02; Fonds d'Innovation Pfizer-FRQS sur la Maladie d'Alzheimer et les Maladies Apparente'es no. 31288; McGill Faculty of Medicine Incentive funding; and an award from The Scottish Rite Charitable Foundation of Canada. The authors declare that they have no conflicts of interest with the contents of this article.

[1] Received an Natural Sciences and Engineering Research Council of Canada Undergraduate Student Research Award (USRA) summer student stipend.

[2] Supported in part by the Freie Universität Berlin within the Excellence Initiative of the German Research Foundation.

[3] To whom correspondence should be addressed: Dept. of Pharmacology and Therapeutics and Cell Information Systems Group, McGill University, Bellini Life Sciences Complex, 3649 Sir-William-Osler Promenade, Montreal, Quebec H3G 0B1, Canada. Tel.: 514-398-2159; E-mail: lisa.munter@mcgill.ca.

[4] The abbreviations used are: PARL, presenilin-associated rhomboid-like protein; APP, amyloid precursor protein; CTF, C-terminal fragment; ER, endoplasmic reticulum; LDL, low-density lipoprotein; LPDS, lipoprotein-deficient serum; S1P, site-1–protease; SREBP, sterol regulatory element-binding protein; bis-tris, 2-[bis(2-hydroxyethyl)amino]-2-(hydroxymethyl)propane-1,3-diol; Tricine, *N*-[2-hydroxy-1,1-bis(hydroxymethyl) ethyl]glycine; PDB, Protein Data Bank; qPCR, quantitative PCR; DMEM, Dulbecco's modified Eagle's medium; FCS, fetal calf serum; PEI, polyethyleneimine; GAPDH, glyceraldehyde-3-phosphate dehydrogenase; CRAC, cholesterol recognition amino acid consensus; TMS, transmembrane sequence.

by signaling through the sterol regulatory element-binding protein 2 (SREBP2). As a result of reduced cellular cholesterol levels, SREBP2 is released from the ER and traffics to the Golgi, and after proteolytic processing, the soluble transcription factor fragment is released, which then translocates to the nucleus to induce gene transcription for cholesterol synthesis (19). Interestingly, APP was previously linked to cholesterol metabolism. The sequence surrounding the APP transmembrane domain, including the G*XXX*G motifs, was shown to bind cholesterol (20–22). Furthermore, APP is able to modulate cholesterol synthesis in an activity-dependent manner in neurons (23). In addition, high cholesterol levels negatively affect AD pathology, leading to increased Aβ levels mediated by sequential β- and γ-secretase cleavages (24–26). Finally, the yeast homologue of RHBDL4, Rbd2, was shown to be involved in lipid homeostasis, too (27, 28). These findings raised the intriguing possibility that RHBDL4-mediated APP processing may be regulated by cholesterol and that RHBDL4 activity in general could be modulated by membrane cholesterol levels. Here, we show evidence that increasing cellular cholesterol levels leads to decreased RHBDL4 activity as determined by decreasing levels of RHBDL4-specific APP fragments, but decreasing cholesterol levels show increased RHBDL4 activity. Furthermore, RHBDL4 itself seems to be able to bind cholesterol via its transmembrane helices. This may transmit cholesterol-dependent regulation of RHBDL4 activity.

Results

Modulating cellular cholesterol levels alters RHBDL4-mediated APP processing

HEK 293T cells endogenously express APP, and we were previously able to show that upon expression of RHBDL4, large endogenous APP CTFs between 10 and 25 kDa in size are generated (9). Those APP CTFs are specific for RHBDL4 and are not generated or degraded by other proteases. We took advantage of this paradigm and used the generation of endogenous APP CTFs as a measure of RHBDL4 activity to study its regulatory mechanisms.

We first transfected HEK 293T cells with RHBDL4 and respective controls, and treated cells with either simvastatin or low-density lipoprotein (LDL) particles for 24 or 48 h, respectively. Simvastatin is a Food and Drug Administration-approved drug to lower cholesterol synthesis by inhibiting hydroxy-3-methylglutaryl–CoA reductase, the rate-limiting enzyme of cholesterol synthesis (29). Thus, simvastatin supplementation is an established treatment to decrease cellular cholesterol levels. Conversely, LDL transports and distributes cholesterol throughout the organism and is taken up by cells through receptor-mediated endocytosis, hence leading to increased cellular cholesterol levels (30, 31).

We found that lowering cholesterol levels upon statin treatment led to a time-dependent increase in 20–25-kDa large CTFs (1.59-fold at 24 h and 5.33-fold at 48 h, see Fig. 1, *A–C*). As observed previously (9), the CTFs derived from classical α- or β-secretase cleavages (see Fig. 1*A*, indicated with a *yellow arrow*) often co-migrate together with a slightly larger 9-kDa RHBDL4-mediated APP CTF, so that this RHBDL4-specific CTF is hard to differentiate from the α/β-CTFs (8 kDa). Furthermore, the anticipated treatment effects on α/β-CTFs have been shown to be oppositional, adding an extra layer of complexity. Although the α-CTF was shown to be increased upon decreased cholesterol levels, the β-CTF was shown to be decreased (32–36). Statin treatment in combination with LPDS is known to not only reduce cholesterol levels but also isoprenoid levels (37). This treatment paradigm was previously shown to accumulate APP intracellularly in the trans-Golgi network and ER (37). The observed overall decrease in α/β-CTFs in all statin-treated samples, could therefore be due to a compartmentalization effect. As the gel resolution does not allow for the detection of an anticipated simultaneous increase of the RHBDL4-mediated 9-kDa APP–CTF due to the aforementioned co-migration, we only quantified RHBDL4-specific fragments with sizes between 20 and 25 kDa (see above). In addition, we quantified full-length APP levels, which revealed a significant increase at 24 and 48 h as well (2.03- and 4.86-fold, respectively). It has been reported that isoprenoids are required for APP trafficking through the secretory pathway (37). To evaluate whether the observed increases in RHBDL4-mediated 20–25-kDa CTFs are due to defects in APP trafficking or due to modulation of RHBDL4 activity, we co-treated simvastatin-treated cells with 0.25 mM mevalonate according to Cole *et al.* (37). At 24 and 48 h, co-treatment with mevalonate rescued APP trafficking and normalized APP full-length level to control levels at both time points. Interestingly, at 24 h we still observe a 1.48-fold ($p = 0.089$) increase in 20–25-kDa CTFs (Fig. 1*G*), which is comparable with results obtained without mevalonate (compare Fig. 1, *C* and *G*). Co-treatment of simvastatin with mevalonate for 48 h showed a trend toward increased CTF levels (1.75-fold ($p = 0.24$), Fig. 1*H*). Overall, decreasing cholesterol levels by statins increased RHBDL4-specific APP CTFs in large part because of altered APP trafficking and higher substrate availability. However, rescuing APP trafficking upon co-treatment with mevalonate still revealed trends toward increased levels of RHBDL4-specific APP CTFs. We therefore sought to use other cholesterol altering methods to substantiate our results.

To increase the cellular cholesterol levels, we treated cells with LDL. However, the effects of LDL treatment on α/β-CTF in cell culture were not fully established. Overall, in our experimental set up, the effects on α/β-CTF are minimal with a trend toward decreased levels. As for the RHBDL4-specific 20–25-kDa APP–CTFs, we observed a trend toward decreased levels after 24 h of LDL treatment (Fig. 1*D*), which became a significant decrease after 48 h (Fig. 1, *E* and *F*). In neither case did we observe a concomitant decrease of full-length APP levels, suggesting that APP trafficking was not affected in these treatments. Thus, lowering cellular cholesterol levels seemed to stimulate RHBDL4-mediated APP cleavages, whereas elevated cholesterol levels decreased RHBDL4-mediated processing. Furthermore, we tested whether a co-treatment of simvastatin together with LDL would be able to rescue the simvastatin-mediated increase in APP CTFs (Fig. 2*A*). Indeed, co-treatment with LDL was able to normalize the increase in APP CTFs caused by simvastatin. It should be noted that mechanistically, simvastatin leads to an overall decrease in cellular cholesterol

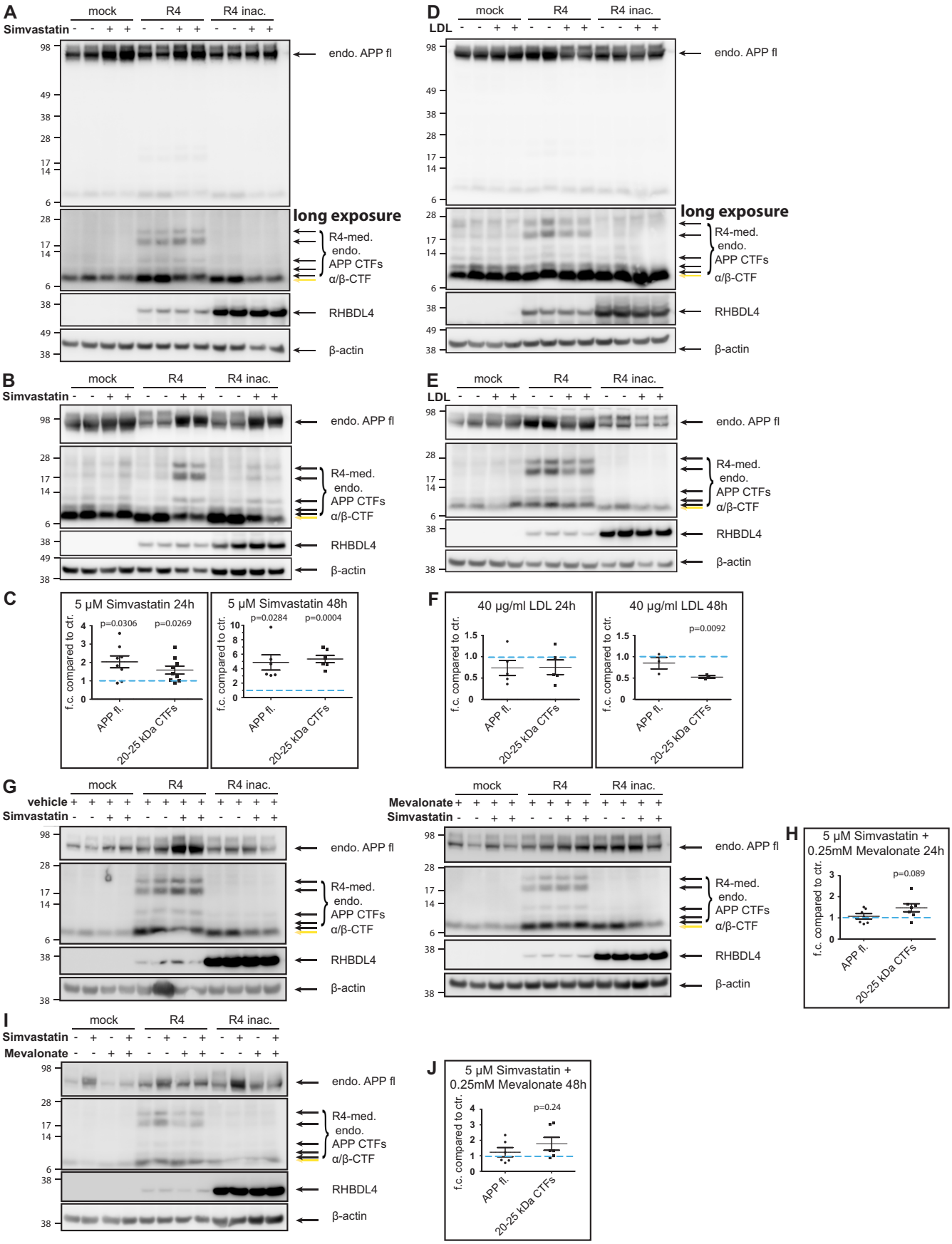
A
mock
R4
R4 inac.
Simvastatin
endo. APP fl
long exposure
R4-med.
endo.
APP CTFs
α/β-CTF
RHBDL4
β-actin
B
C
5 µM Simvastatin 24h
5 µM Simvastatin 48h
f.c. compared to ctr.
p=0.0306
p=0.0269
p=0.0284
p=0.0004
APP fl.
20-25 kDa CTFs
D
LDL
E
F
40 µg/ml LDL 24h
40 µg/ml LDL 48h
p=0.0092
G
vehicle
H
5 µM Simvastatin +
0.25mM Mevalonate 24h
p=0.089
I
Mevalonate
J
5 µM Simvastatin +
0.25mM Mevalonate 48h
p=0.24

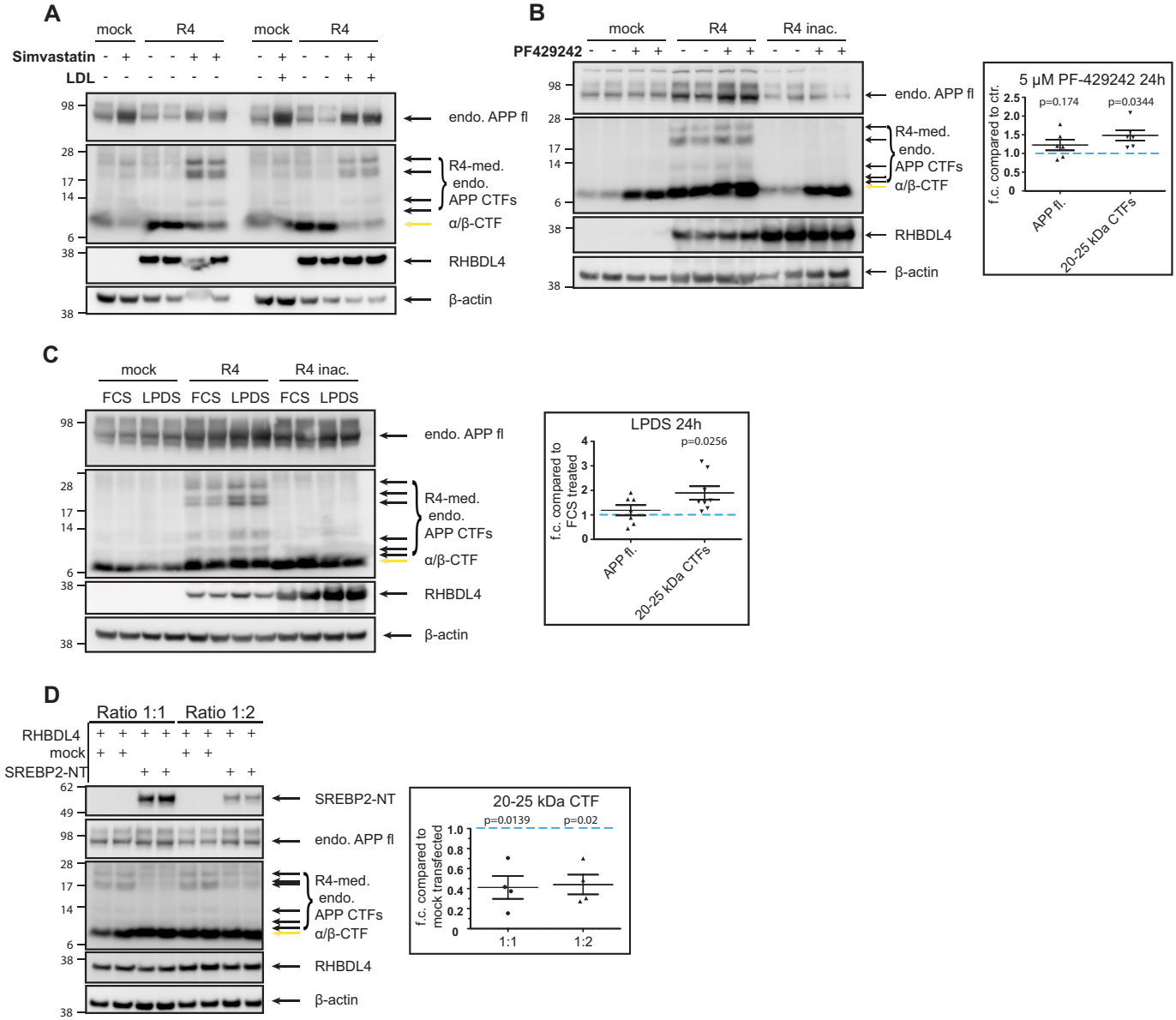

Figure 2. Alterations of cellular cholesterol levels lead to changes in RHBDL4-mediated endogenous APP CTF levels. *A,* co-treatment of simvastatin and LDL partially rescues the effects of simvastatin alone. Experiments were performed as in *C* and *D*; however, 36 h post-transfection, cells were either treated with 5 μM simvastatin alone or co-treated with 40 μg/ml LDL for 48 h. Co-treatment led to reduced simvastatin-mediated increase in 20–25-kDa APP CTFs. *B,* RHBDL4-mediated endogenous APP CTFs were analyzed upon treatment with site-1–protease inhibitor PF429242 in HEK 293T cells. 36 h post-transfection, cells were treated with 5 μM inhibitor for 24 h, and DMSO was used as vehicle control. Representative Western blotting of five independent experiments is shown. *C,* comparison of the effects of FCS *versus* LPDS on RHBDL4-mediated generation of APP CTFs. Cells were treated with 10% FCS or 10% LPDS in DMEM for 24, 12, to 36 h post-transfection. Representative Western blotting of seven independent experiments is shown. *D,* co-transfection of RHBDL4 and constitutively active N-terminal domain of SREBP2 (SREBP2-NT) in different ratios as indicated. Representative Western blotting of four independent experiments is shown. *B–D,* in all cases, endogenous APP CTFs and APP full length were quantified with ImageJ similar to Fig. 1. All values were first normalized to β-actin and then the fold change (*f.c.*) was calculated compared with vehicle-treated (*A*), FCS-treated (*B*), or mock-transfected (*D*) samples for RHBDL4-transfected samples. Control was always set to 1 in each individual experiment (*blue dashed line*). Mean ± S.E. is depicted, $n = 4–7$, p values for Holm-Bonferroni corrected one sample *t* test are reported. *A–D,* detection of APP full length and endogenous CTFs with Y188 if not indicated otherwise; RHBDL4 with anti-Myc antibody, and β-actin as a loading control.

Figure 1. Simvastatin increases RHBDL4-mediated APP processing, whereas LDL decreases it. *A, B, D, E, G,* and *I,* analysis of endogenous (*endo.*) APP CTF in HEK 293T cells. Transient transfection of mock, RHBDL4 active (*R4*), or inactive (*inac.*) resulted in generation of multiple RHBDL4-mediated endogenous APP CTFs between 8 and 25 kDa. 36 h post-transfection, cells were either treated with 5 μM simvastatin alone, 40 μg/ml LDL, or 5 μM simvastatin together with 0.25 mM mevalonate for 24 h (*A, D,* and *G*) or 48 h (*B, E,* and *I*), respectively. DMSO or water was used as vehicle control. Representative Western blottings of 3–9 independent experiments are shown. *fl,* full-length. *C, F, H,* and *J,* for quantification of endogenous APP CTFs and APP full-length, the signals between 20 and 25 kDa (indicated by *upper two arrows*) and endogenous full-length APP were quantified with ImageJ. All values were first normalized to β-actin, and then the fold changes (*f.c.*) compared with vehicle-treated samples were calculated for RHBDL4-transfected samples. Vehicle control was set to 1 in each individual experiment (*blue dashed line*). Mean ± S.E. is depicted, $n = 3–9$, p values for Holm-Bonferroni–corrected one sample *t* test are reported. *A–D, G,* and *H,* detection of APP full length and endogenous CTFs with Y188 if not indicated otherwise; RHBDL4 with anti-Myc antibody, and β-actin as a loading control.

levels, presumably in all cellular membranes, including the ER membrane, whereas the uptake of LDL predominantly leads to an increase in membrane cholesterol along the route of its uptake (*i.e.* plasma membrane, endosome, and lysosome) and affects the ER to a lesser extent. Therefore, and to substantiate the idea that cellular cholesterol levels impact the activity of RHBDL4, we performed additional experiments using other strategies to increase or decrease cholesterol levels.

Site-1–protease (S1P) is the sheddase in the regulated intramembrane proteolysis process of liberating transcriptionally active SREBPs from the membrane (38). Consequently, S1P inhibition was shown to decrease endogenous cholesterol synthesis by reducing transcriptional activation of the synthesis machinery (39). Treatment of cells with the S1P inhibitor PF429242 led to a 1.49-fold increase in the 20–25-kDa RHBDL4-mediated APP CTFs, paralleling the results of the simvastatin treatments (Fig. 2*B*). Interestingly, we observed an increase in the 8-kDa CTF, not only in the RHBDL4 co-expression but also in the mock and inactive RHBDL4 controls, implying that this signal may be mainly due to heightened α-secretase activity as mentioned previously. Importantly, the S1P inhibitor does not affect full-length APP levels (determined by quantification of APP full length) or maturation of APP contrary to statins that affect translocation of mature APP to the plasma membrane. Hence, differences in the mechanism as to how each inhibitor functions may explain the results obtained. Based on our findings, we can speculate that the S1P inhibitor does not affect isoprenoid levels, and therefore the results are meaningful with regard to effects mediated by cholesterol.

To further corroborate the idea that decreasing cellular cholesterol levels stimulate RHBDL4 activity, we searched for an assay that did not require the use of a drug. Incubation with FCS deprived of lipoproteins (lipoprotein-deficient serum, LPDS) leads to decreased cellular cholesterol content (37, 40, 41). We therefore simply compared the effect of FCS *versus* LPDS on RHBDL4-mediated APP processing. Compared with FCS, LPDS increased the levels of 20–25-kDa CTFs 1.90-fold, in line with the results observed for simvastatin and S1P treatments (Fig. 2*C*). Furthermore, we observed an increase in 10–12-kDa CTFs together with a decrease in α/β-CTF (the latter is best observed in the mock-treated samples). There was no change in APP full-length levels observed under these conditions.

Finally, we performed a series of transfections with a constitutively active SREBP2 form, which will lead to continued transcriptional activation of the cholesterol synthesis machinery, and thus it elevates the cellular cholesterol content (42). Indeed, overexpression of this constitutively active transcription factor almost completely represses the generation of RHBDL4-mediated 20–25-kDa CTFs as indicated by a 0.4-fold change in signal as compared with control (Fig. 2*D*). Different ratios of RHBDL4 to SREBP2 did not show a dose-response effect, suggesting an all-or-none effect within our experimental timeline. Furthermore, the signal at 8 kDa was increased with active SREBP2 implying that this fragment derived predominantly from β-secretase cleavages (it was not further analyzed). Overall, these results supported the idea that increasing levels of cholesterol negatively impact the activity of RHBDL4, but decreasing cellular cholesterol levels trigger RHBDL4 activity.

Cholesterol binding– deficient APP mutants are processed similar to APP WT

There has been a large body of work showing that APP itself can bind cholesterol. Considering that RHBDL4-mediated APP processing seems to be modulated by cholesterol, we delved into the question of whether direct binding of cholesterol to APP regulates substrate recognition. Barrett *et al.* (20) showed that substitution of selected amino acids to alanine completely abrogates cholesterol binding, *i.e.* F20A, E22A, I32A, G29A, G33A, and V39A, highlighted in Fig. 3*A*. Substitutions F19A and S26A only weakly affect cholesterol binding and are expected to have mild effects on RHBDL4 processing. We generated this set of APP mutants and analyzed the cleavage efficiency of RHBDL4. Please note that because RHBDL4 cleaves APP in the ER, full-length APP as well as the 70-kDa ectodomain fragment were detected in the cell lysate. The results revealed that all APP mutants are processed with similar efficiency as compared with WT APP, when analyzing the anticipated decrease in APP full length as well as the APP CTFs (Fig. 3, *B–D*). Two APP mutants, however, stood out. The APP F19A/F20A/E22A mutant showed a trend toward increased levels of RHBDL4-mediated CTFs, although not significant (Fig. 3*E*). Furthermore, this mutant actually showed an additional 6e10-reactive CTF at 7 kDa, which may suggest that loss of cholesterol binding in this case decreased the specificity of the enzyme or that an additional cleavage site was generated through the mutation. Finally, the triple mutant G29A/G33A/V39A showed significantly less RHBDL4-mediated CTFs than the WT, contrary to our expectations. It is possible that these three mutations prevent substrate recognition by RHBDL4, but they might also alter the half-life of the fragments. Overall, the results suggest that direct binding of cholesterol to APP does not lead to alterations in RHBDL4-mediated APP processing.

Does cholesterol directly bind to RHBDL4?

Based on the results so far, we considered the possibility that cholesterol may bind directly to RHBDL4 and thereby modulate the enzyme's activity. Two consensus sequences for cholesterol-binding sites have been described. The cholesterol recognition amino acid consensus sequences (CRAC) ((L/V)$X_{(1-5)}$Y$X_{(1-5)}$(R/K)) and its "mirror code" CARC ((R/K)$X_{(1-5)}$(Y/F)$X_{(1-5)}$(L/V)) (43). Although the predictive nature of these consensus sequences has not been well established, it is known that they are found in a great variety of proteins that were shown to bind cholesterol such as the acetylcholine receptor (44) or mouse caveolin (45). Moreover, amino acid exchange of the central tyrosine residue was reported to completely abrogate cholesterol binding (45, 46). After screening the RHBDL4 amino acid sequence, several potential CRAC and CARC motifs were identified (Fig. 4*A*).

To determine whether such motifs would allow binding of cholesterol, we first generated a homology model of RHBDL4 (Fig. 4*B*). Based on this model, we found that the motifs in helix 3 containing Tyr-106 and in helix 6 containing Tyr-205 align within a transmembrane sequence of RHBDL4. Also, Tyr-106 and Tyr-205 almost oppose each other in the homology model, suggesting the possibility that binding of cholesterol to these

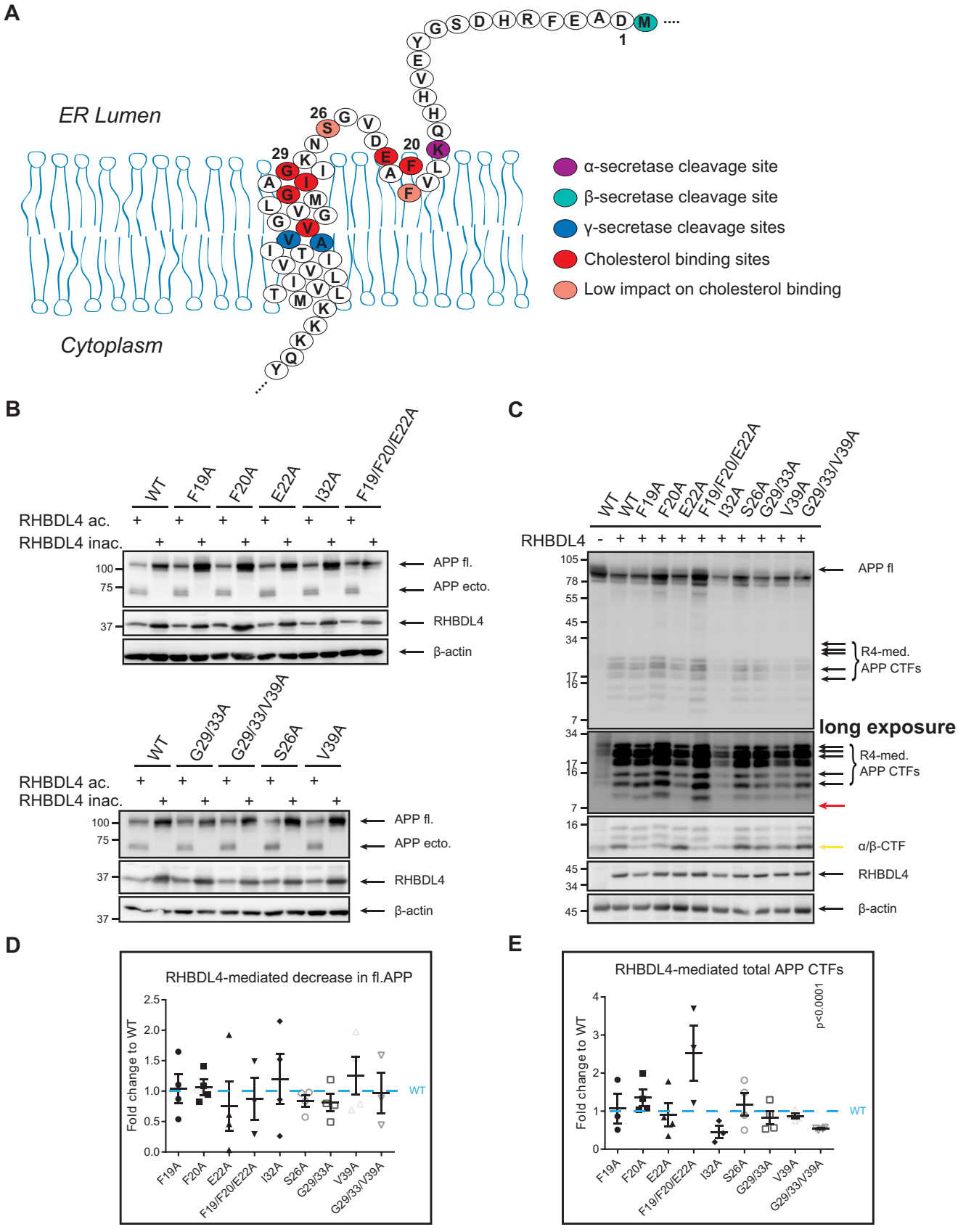
A
ER Lumen
Cytoplasm
α-secretase cleavage site
β-secretase cleavage site
γ-secretase cleavage sites
Cholesterol binding sites
Low impact on cholesterol binding
B
WT
F19A
F20A
E22A
I32A
F19/F20/E22A
RHBDL4 ac.
RHBDL4 inac.
APP fl.
APP ecto.
RHBDL4
β-actin
G29/33A
G29/33/V39A
S26A
V39A
C
RHBDL4
APP fl
R4-med.
APP CTFs
long exposure
α/β-CTF
D
RHBDL4-mediated decrease in fl.APP
Fold change to WT
E
RHBDL4-mediated total APP CTFs
p<0.0001

two helices could put conformational constraint on the enzyme and thus perhaps transmit signals toward the active center of the enzyme as initially proposed for GlpG (Fig. 4*B*) (47). Interestingly, the CARC motif in transmembrane helix 6 is conserved between 72 species with Tyr-205 being conserved to 100% between species indicating that this motif, or at least the tyrosine residue, is important for the function of the enzyme (Fig. 4*C*). Similarly, the degree of conservation of Tyr-106 over 72 species was 81.7% (data not shown). We therefore replaced Tyr-106 and Tyr-205 with alanine and anticipated that the mutations should abrogate cholesterol binding. Hence, one would expect enhanced enzyme activity as observed for the statin, S1P inhibitor, and LPDS treatments. Expression of either RHBDL4 Y106A, Y205A, or Y106A/Y205A mutant led to significant increases in 20–25-kDa endogenous APP CTFs as compared with WT (1.72-, 2.04-, and 1.76-fold compared with WT, respectively). Similarly, we observed an increase in 8–12-kDa fragments for all tyrosine mutants, implying that in this experimental set up the signal is mostly derived from RHBDL4 activity. Notably, endogenous APP full-length levels increased as well upon transfection of RHBDL4 mutants when compared with WT RHBDL4 (Fig. 4*D*, Y106A, 1.23-fold; Y205A, 1.72-fold; and Y106A/Y205A, 1.6-fold). These changes, however, are not due to an increase in APP mRNA levels compared with RHBDL4 WT-transfected cells (Fig. 4*F*).

To further corroborate that the RHBDL4 mutants are deficient in cholesterol binding, we reasoned that the RHBDL4 mutants should be unresponsive to LPDS treatment and thus should not increase APP CTFs compared with FCS. We performed these experiments with a slightly different treatment paradigm, where we started a 24-h treatment 12 h post-transfection as RHBDL4 mutants seemed to be slightly less stable than wild type (WT). As shown in Fig. 4*G*, LPDS treatment increased the 20–25-kDa CTFs in RHBDL4 WT-expressing cells as compared with FCS, although not statistically significant anymore due to the altered treatment paradigm (Fig. 4*G*). Surprisingly, we also noted an overall increase in 8–12-kDa CTFs, fitting our observation from Fig. 2*C* that α/β-CTFs co-migrate with an RHBDL4-mediated CTF. Importantly, the increase in 20–25-kDa APP CTFs upon LPDS treatment was completely abolished for the Y106A mutant as well as the double mutant Y106A/Y205A. The single mutant RHBDL4 Y205A seems to still be responsive to cholesterol but to a lesser extent than WT (Fig. 4*H*). Finally, we performed pulldown experiments with biotinylated cholesterol and neutravidin beads, assuming that RHBDL4 WT would be precipitated with cholesterol, although the mutants would not. As shown in Fig. 4*I*, RHBDL4 WT precipitated specifically in samples that were incubated with cholesterol, although Y106A and Y205A did not precipitate. The double mutant Y106A/Y205A was pulled down with cholesterol to a lesser extent than WT, but it also precipitated in the sample where no cholesterol was added. In summary, our data support the intriguing possibility that RHBDL4 binds cholesterol and that this interaction regulates RHBDL4 activity.

Discussion

Human rhomboid proteases have been vastly understudied when it comes to the study of intramembrane proteases, mostly due to the lack of known substrates with proven *in vivo* relevance or useful tools such as recombinant expression system or inhibitors to study their kinetics or mechanisms of action (48). Our recent finding that APP is exceptionally well cleaved by RHBDL4 in its ectodomain enabled us to use this robust cleavage as an indirect readout for RHBDL4 activity (9).

Here, we describe a potential mechanism of regulation for a human rhomboid protease. Upon various different treatments and transfection schemes, we were able to show that lowering cellular cholesterol levels leads to an increase in RHBDL4-mediated APP CTF levels, indicating enhanced RHBDL4 activity. Conversely, increasing cellular cholesterol levels led to a decrease in RHBDL4-mediated APP–CTFs and hence a decrease in RHBDL4 activity. With RHBDL4 localizing to the ER, it is further assumed that changes in cellular cholesterol levels will lead to changes in ER cholesterol levels (49); however, determining ER cholesterol levels has proven challenging and beyond the scope of this paper.

Simvastatin treatment in lipoprotein-deficient serum does not only reduce cholesterol levels but also isoprenoid levels, leading to changes in trafficking through the secretory pathway (37). This may explain the observed accumulation of immature full-length APP upon simvastatin treatment and the concomitant decrease in α- and β-CTFs. To circumvent these effects, we co-treated the samples with mevalonate and were able to fully rescue APP trafficking defects. Furthermore, we still observed trends toward increased levels of RHBDL4-mediated APP CTFs. The mevalonate co-treatment enabled us to discriminate between APP trafficking-mediated effects on CTF generation and cholesterol-dependent effects. Furthermore, no effects on APP full-length levels were observed for S1P inhibitor or LPDS treatment. Overall, we conclude that all three cholesterol-lowering assays increased RHBDL4 activity to a similar extent. In contrast, different assays with the aim to increase cellular cholesterol levels showed decreased levels of RHBDL4-mediated APP CTFs, suggesting decreased RHBDL4 activity upon high cellular cholesterol content. Interestingly, in the mock-treated samples, we observed a time-dependent decrease in α/β-CTF

Figure 3. Cholesterol binding–deficient APP mutants are processed by RHBDL4 similar to WT. *A,* scheme of the APP transmembrane region as well as α-, β-, and γ-secretase cleavage sites. Binding sites for cholesterol in APP are highlighted; substitution to alanine either abrogates cholesterol binding (*red*) or only weakly affects it (*light red*) according to Barrett *et al.* (20). *B* and *C,* analysis of processing of cholesterol binding–deficient APP mutants compared with APP WT. Co-transfection of RHBDL4 active or inactive with APP cholesterol binding–deficient mutants. Samples were analyzed regarding full-length APP levels, APP ectodomain (*ecto*). fragment (both in *B*), as well as RHBDL4-mediated CTFs (*C*). Detection of APP full length and APP ectodomain was performed with 22C11, CTFs with either 6e10 (*upper two panels* in *B*), or anti-FLAG. RHBDL4 detected with anti-Myc antibody and β-actin as a loading control. *D* and *E,* decrease in full-length APP was quantified and compared with WT (80%) (9) and taken as a measure of processing efficiency. Full-length levels (*D*) were quantified, normalized to β-actin, calculated as % of inactive, and then displayed as fold change compared with WT. In a similar fashion, 10–25-kDa APP CTF levels were quantified, normalized to β-actin, and directly compared with WT. Mean ± S.E. is depicted, $n = 3–4$, p values for Holm-Bonferroni corrected one sample t test are reported.

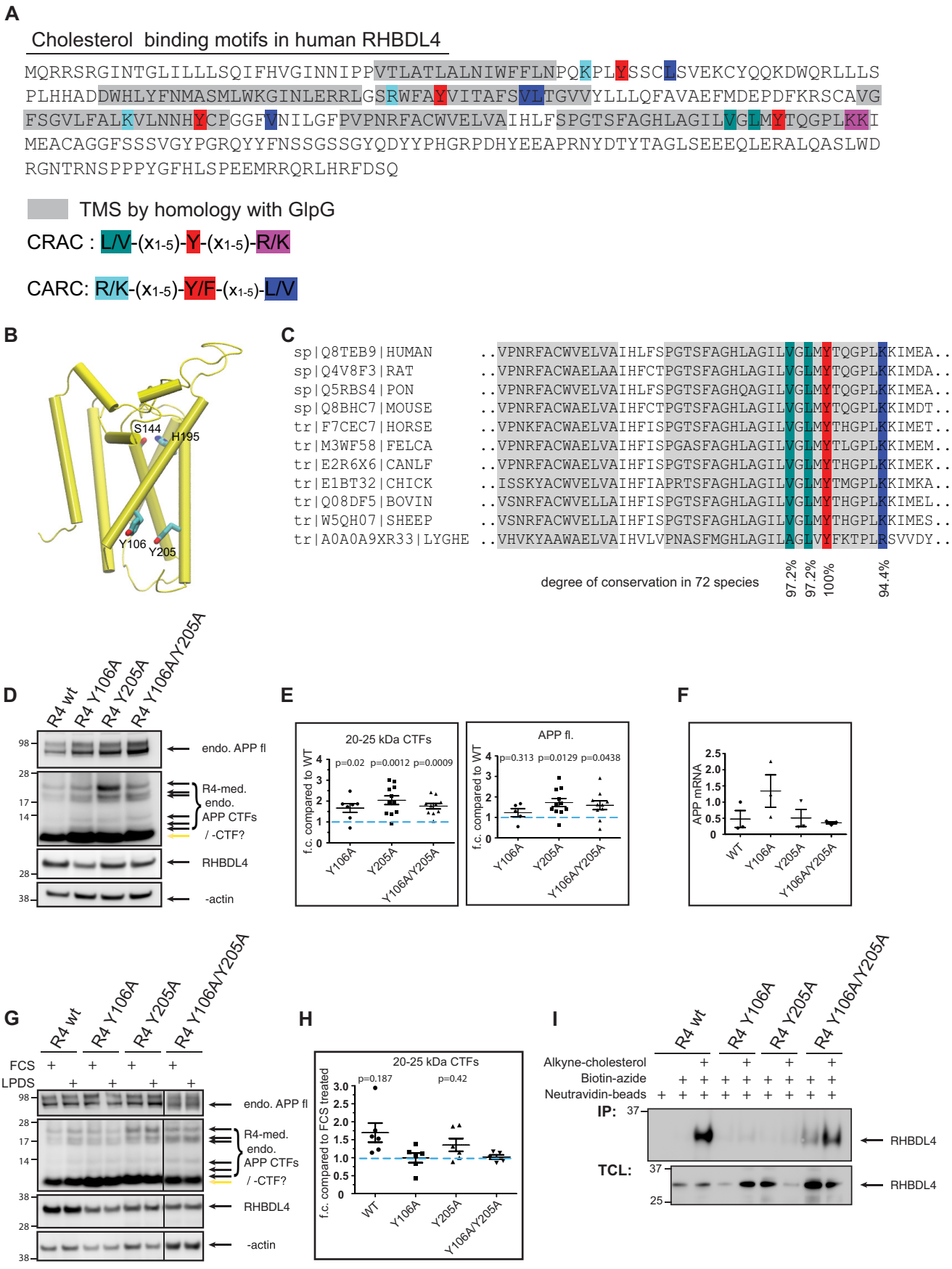
A
Cholesterol binding motifs in human RHBDL4
MQRRSRGINTGLILLLSQIFHVGINNIPPVTLATLALNIWFFLNPQKPLYSSCLSVEKCYQQKDWQRLLLS
PLHHADDWHLYFNMASMLWKGINLERRLGSRWFAYVITAFSVLTGVVYLLLQFAVAEFMDEPDFKRSCAVG
FSGVLFALKVLNNHYCPGGFVNILGFPVPNRFACWVELVAIHLFSPGTSFAGHLAGILVGLMYTQGPLKKI
MEACAGGFSSSVGYPGRQYYFNSSGSSGYQDYYPHGRPDHYEEAPRNYDTYTAGLSEEEQLERALQASLWD
RGNTRNSPPPYGFHLSPEEMRRQRLHRFDSQ
TMS by homology with GlpG
CRAC : L/V-(x1-5)-Y-(x1-5)-R/K
CARC: R/K-(x1-5)-Y/F-(x1-5)-L/V
B
S144
H195
Y106
Y205
C
sp|Q8TEB9|HUMAN ..VPNRFACWVELVAIHLFSPGTSFAGHLAGILVGLMYTQGPLKKIMEA..
sp|Q4V8F3|RAT ..VPNRFACWAELAAIHFCTPGTSFAGHLAGILVGLMYTQGPLKKIMDA..
sp|Q5RBS4|PON ..VPNRFACWVELVAIHLFSPGTSFAGHQAGILVGLMYTQGPLKKIMEA..
sp|Q8BHC7|MOUSE ..VPNRFACWAELVAIHFCTPGTSFAGHLAGILVGLMYTQGPLKKIMDT..
tr|F7CEC7|HORSE ..VPNKFACWAELVAIHFISPGTSFAGHLAGILVGLMYTHGPLKKIMET..
tr|M3WF58|FELCA ..VPNRFACWAELVAIHFISPGASFAGHLAGILVGLMYTLGPLKKIMEM..
tr|E2R6X6|CANLF ..VPNRFACWAELVAIHFISPGTSFAGHLAGILVGLMYTHGPLKKIMEK..
tr|E1BT32|CHICK ..ISSKYACWVELVAIHFIAPRTSFAGHLAGILVGLMYTMGPLKKIMKA..
tr|Q08DF5|BOVIN ..VSNRFACWVELLAIHFISPGTSFAGHLAGILVGLMYTHGPLKKIMEL..
tr|W5QH07|SHEEP ..VSNRFACWVELLAIHFISPGTSFAGHLAGILVGLMYTHGPLKKIMES..
tr|A0A0A9XR33|LYGHE ..VHVKYAAWAELVAIHVLVPNASFMGHLAGILAGLVYFKTPLRSVVDY..
degree of conservation in 72 species
97.2%
97.2%
100%
94.4%
D
R4 wt
R4 Y106A
R4 Y205A
R4 Y106A/Y205A
98
28
17
14
28
38
endo. APP fl
R4-med. endo. APP CTFs / -CTF?
RHBDL4
-actin
E
20-25 kDa CTFs
p=0.02 p=0.0012 p=0.0009
f.c. compared to WT
Y106A
Y205A
Y106A/Y205A
APP fl.
p=0.313 p=0.0129 p=0.0438
F
APP mRNA
WT
Y106A
Y205A
Y106A/Y205A
G
R4 wt
R4 Y106A
R4 Y205A
R4 Y106A/Y205A
FCS + + + +
LPDS + + + +
98
28
17
14
38
28
38
endo. APP fl
R4-med. endo. APP CTFs / -CTF?
RHBDL4
-actin
H
20-25 kDa CTFs
p=0.187
p=0.42
f.c. compared to FCS treated
WT
Y106A
Y205A
Y106A/Y205A
I
R4 wt
R4 Y106A
R4 Y205A
R4 Y106A/Y205A
Alkyne-cholesterol + + + +
Biotin-azide + + + + + + + +
Neutravidin-beads + + + + + + + +
IP:
TCL:
37
37
25
RHBDL4
RHBDL4

upon LDL treatment that might reflect an effect on APP trafficking rather than effects on the secretase themselves.

It is important to note that the physiological role of RHBDL4-mediated APP CTFs is currently not clear, and further investigation may be interesting considering the recently increasing interest in large APP CTFs as precursors of novel Aη fragments (50, 51). Additionally, it is interesting to note that elevated cholesterol levels are known to increase Aβ levels, whereby our data suggest that RHBDL4 activity will be decreased under these conditions. Conversely, activating RHBDL4 by lowering cholesterol levels could decrease Aβ levels, assuming that full-length APP would be degraded in the ER by RHBDL4 circumventing its trafficking to the plasma membrane. Thus, RHBDL4-mediated APP processing may be pronounced under low cholesterol conditions, whereas high cellular cholesterol levels would drive amyloidogenic APP processing.

It has been demonstrated using nuclear magnetic resonance (NMR) that the transmembrane sequence (TMS) of APP binds cholesterol through direct interactions of cholesterol with selected amino acids (20, 21). Amino acid exchanges at these positions to alanine abrogate binding (as indicated in Fig. 3*A*). To answer the intriguing question whether or not the cholesterol sensitivity of the RHBDL4–APP processing pathway is mediated directly by APP, we anticipated that binding of cholesterol to APP might be necessary to either mediate specificity, orient the enzyme and substrate correctly toward each other, or restrict access of the substrate to the active center. Therefore, we assumed that cholesterol binding– deficient APP mutants would undergo enhanced RHBDL4-mediated processing. Cleavage efficiency was assessed by analyzing the decrease in APP full-length levels and generation of RHBDL4-specific fragments. Overall, all APP mutants were processed similar to WT in this analysis scheme regarding the published 80% decrease in full-length APP WT, when co-expressed with RHBDL4. Furthermore, we observed similar levels of the APP ectodomain fragment for all APP mutants, indicating that cholesterol binding to APP does not mediate or restrict substrate access to the active center of RHBDL4 and thus does not alter cleavage efficiency. Analysis of the APP–CTF pattern did not reveal striking observations either indicating that cholesterol binding to APP is not involved in orienting the enzyme and substrate. The triple mutant F19A/F20A/E22A showed the appearance of an extra and smaller band that was 6e10-reactive but not FLAG-reactive (the tag sits at the very C terminus) suggesting an additional membrane cleavage by RHBDL4. This observation could be explained by data from Moin and Urban (13) showing that membrane alterations could lead to a loss of cleavage specificity in the case of the bacterial rhomboid GlpG. Finally, the significant decrease in RHBDL4-mediated APP CTFs from the APP triple mutant G29A/G33A/V39A might again argue for a different stability of these CTFs.

Because binding of cholesterol to APP seemed to be a minor factor in mediating the stimulating or repressing effects of cholesterol on RHBDL4 activity, we considered a direct binding of cholesterol to the enzyme. Literature research revealed that specific amino acid sequences known as CRAC, and the mirror version CARC (see Fig. 4*A*), are known motifs, able to bind cholesterol via a TMS or in juxtamembrane regions (43, 45). Screening of the human RHBDL4 sequence exposed multiple potential CRAC and CARC motifs in RHBDL4, hinting toward the intriguing ability of RHBDL4 to bind cholesterol via its TMS. Analysis of all these potential binding motifs in a homology model of RHBDL4 (Fig. 4*B*) suggests that the motif in TMS3 surrounding Tyr-106 and the motif in TMS6 surrounding Tyr-205 are the most likely candidates to bind cholesterol. In either case, all necessary amino acid residues involved in binding cholesterol lined up on one site of the helix (Fig. 4*B*), and the side chains of these groups from both TMS3 and TMS6 are oriented toward the same potential cholesterol-binding cleft. A caveat of our analysis is that we rely on a homology model, and thus the accuracy of the orientation of specific amino acid side chains is difficult to assess. Nevertheless, we suggest that binding of cholesterol at the binding cleft proposed here might restrict the structural dynamics of the enzyme and thereby impair either substrate gating or enzyme activity. Hence, we anticipated that mutations of the necessary tyrosine residues should abrogate cholesterol binding and increase APP cleavage, which we did observe for both single mutants and the double mutant. However, the effect of single mutations compared with the double mutation was not additive, suggesting that mutating a single cholesterol-binding site might affect the overall binding of cholesterol to the cleft. Furthermore, we observed differences in responsiveness to LPDS treatment between these RHBDL4 mutants. RHBDL4 Y106A as well as the double mutant Y106A/Y205A were unresponsive to LPDS

Figure 4. Identification of potential cholesterol-binding motifs in RHBDL4. *A,* human RHBDL4 protein sequence is displayed with the six transmembrane regions highlighted in *gray* (determined by homology with GlpG). Furthermore, potential CRAC motifs and the mirror version (*CARC*) are highlighted. *B,* RHBDL4 homology model based on GlpG crystal structure. The molecular image was generated using Visual Molecular Dynamics (57). Serine 144 and histidine 195 are displayed as *sticks* and form the active center. Tyr-106 in TMS3 and Tyr-205 in TMS6 are highlighted. *C,* comparison of RHBDL4 sequences from a total of 72 species (11 examples displayed here) show a high degree of conservation across species for the CRAC motif in TMS6. *D,* point mutations in RHBDL4 increase protease activity. Tyr-106 and Tyr-205 were mutated to alanine. RHBDL4 mutants were transfected into HEK 293T cells, and the generation of endogenous APP CTFs was determined by Western blot analysis. Representative Western blotting of 7–9 independent experiments is displayed. *F,* analysis of APP mRNA levels upon transfection of RHBDL4 WT, Y106A, Y205A, and Y106A/Y205A. No significant differences for APP mRNA were detected. GAPDH and β-actin served as reference genes. Data are displayed as mean expression ± S.E., $n = 3$. One-way analysis of variance followed by Dunnett's post hoc comparison with WT as control was performed. *G,* RHBDL4 mutants are not responsive to LPDS treatment. 12 h post-transfection, HEK 293T cells were treated with either 10% FCS or LPDS in DMEM for 24 h. A representative Western blotting of six independent experiments is shown. *E* and *H,* APP CTFs or APP full length were quantified, and results were normalized to β-actin and then either compared with WT (*D*) or FCS treatment (*F*). *D,* WT was set to 1 and is indicated by the *blue dashed line*, and *F,* FCS-treated samples were set to 1. Mean ± S.E. are displayed, $n = 6–9$ as stated above, p values for Holm-Bonferroni corrected one sample t test are reported. *I,* pulldown of RHBDL4 with biotinylated cholesterol. RHBDL4 WT and mutants were transfected, and membrane preparations were incubated with alkyne-cholesterol. After clicking biotin-azide to cholesterol, a neutravidin pulldown was performed. Total cell lysates were collected before the click chemistry was performed, and the Western blotting shows expression of RHBDL4 WT and mutants. Representative Western blots of 3–4 independent experiments are shown. *D, F,* and *I,* detection of APP full length and endogenous CTFs with Y188, RHBDL4 with anti-Myc antibody, and β-actin as a loading control.

treatment, *i.e.* we observed no increase in APP CTF as compared with WT RHBDL4. RHBDL4 Y205A showed an attenuated response as compared with WT RHBDL4. Please note that due to the altered treatment paradigm in Fig. 4*G* compared with Fig. 2*C*, and the consequently reduced effect size, we only observed trends. The attenuation could possibly be explained by different π interactions of this residue with Trp-103 in helix 3, as suggested by our homology model. In addition, we noticed that the expression of RHBDL4 Y205A and Y106A/Y205A significantly increased endogenous APP full-length levels, whereas APP mRNA levels are unaltered (Fig. 4*F*). These results seem to suggest secondary effects of these RHBDL4 mutants. It is possible that the APP–RHBDL4 pair acts as a cholesterol sensor and regulates RHBDL4-mediated APP processing, and trafficking is required for cholesterol homeostasis. It should be mentioned here that a recent publication suggested a role for RHBDL4 in the ER export of proteins (16), which could be relevant for APP as well. RHBDL4 mutants may be defective in mediating ER export of proteins and therefore show accumulation of immature APP. Thus, cholesterol binding to RHBDL4 might not only alter its proteolytic activity, but perhaps also its chaperoning activity.

To substantiate the idea that RHBDL4 indeed binds cholesterol, we performed cholesterol pulldown experiments. As expected, these experiments imply a strong interaction between RHBDL4 WT and cholesterol, whereas Y106A and Y205A could not be pulled down with biotinylated cholesterol. The double mutant Y106A/Y205A was precipitated without cholesterol present, suggesting unspecific interactions with the beads. This might be indicative of a less stable folding of this mutant or an exposition of hydrophobic residues. However, this mutant consistently showed a slightly stronger signal for RHBDL4 upon cholesterol pulldown as compared with the negative control, which may derive from unspecified interactions with cholesterol. Overall, only RHBDL4 WT precipitated strongly and specifically with biotinylated cholesterol, as anticipated.

Finally, we analyzed the degree of conservation between species for these cholesterol-binding motifs in RHBDL4, showing high percentages for the CRAC motif in TMS6 (between 95 and 100% for all necessary amino acids) and above 80% for the tyrosine of the CARC in TMS3.

Overall, our data imply the captivating possibility that RHBDL4 itself can bind cholesterol via its TMS and that cholesterol binding in turn could mediate substrate gating or recognition and regulate enzyme activity. So far, the crystal structures for bacterial homologues indicated substrate gating without the involvement of TMS3 or TMS6. However, modeling data from Bondar *et al.* (47) suggested that multiple hydrogen bonds along helix 3 of GlpG might be necessary to couple the L1 loop to TMS2/5 and that remote structures such as the rigid TMS3 might be important for enzyme activity. In this regard, binding of cholesterol to TMS3 of RHBDL4 might add rigidity to the enzyme, which may explain why abrogation of cholesterol binding increased the enzyme's activity.

Finally, it has to be noted that our readout of activity has been the RHBDL4-mediated generation of APP CTFs, and we cannot rule out that some effects in part are mediated by APP itself, especially considering that APP was proposed as an upstream regulator of transcriptional repression of cholesterol synthesis (23). Pierrot *et al.* (23) suggested that the interaction of APP with SREBP prevented its processing by site-2 protease, thereby reducing overall cholesterol synthesis. Consequently, cholesterol levels in the ER would drop, and this would, according to our data presented herein, lead to RHBDL4 activation and APP degradation, which would then allow SREBP2 processing again to induce cholesterol synthesis. This potential interaction cycle has, however, to be investigated experimentally. Overall, our findings suggest that RHBDL4 itself may act as a cholesterol sensor in the ER. It will be interesting to reveal how this regulation may be connected to APP processing *in vivo*.

Conclusion

Here, we showed that membrane cholesterol can alter the activity of a human rhomboid protease, RHBDL4. Our results demonstrated that cholesterol diminishes RHBDL4 activity implying that the steroid backbone may constitute a starting point for the development of RHBDL4 inhibitors. Because there is currently a lack of selective and efficacious inhibitors for mammalian rhomboid proteases, our results might prove useful with regard to the development of inhibitors.

Materials and methods

DNA constructs

Plasmid pCMV6 containing cDNA encoding for human RHBDL4 with a C-terminal Myc-FLAG tag was obtained from OriGene. Inactive RHBDL4 S144A was generated by site-directed mutagenesis using the forward primer 5′-GCTGTAGGTTTCGCAGGAGTTTTGTTT-3′ and the reverse primer 5′-AAACAAAACTCCTGCGAAACCTACAGC-3′. Mutants deficient in cholesterol binding, namely RHBLD4 Y106A, RHBDL4 Y205A, and RHBDL4 Y106/205A, were cloned using gene blocks from IDT. Specifically, gene blocks were dissolved in H_2O at a concentration of 10 ng/μl, of which 4 ng/μl DNA were digested using XbaI and XmaI restriction enzymes. Enzymes were subsequently heat-inactivated at 65 °C for 20 min, and samples were ready for ligation. 1 μg of pCMV6 vector encoding hRHBDL4 cDNA plasmid was digested using the same restriction enzymes, treated with alkaline phosphatase to avoid re-ligation of the vector, and purified from gels. With 50 ng of the vector, the digested gene blocks were ligated at different vector-to-insert ratios using T4 DNA ligase (New England Biolabs) at room temperature overnight (16–18 h). The ligation samples were pooled and transformed via heat shock. Cells were plated on kanamycin agar plates and incubated overnight at 37 °C. DNA constructs of single colonies were then purified (Qiagen), and full sequences were confirmed using DNA sequencing by Genome Quebec. Untagged APP695 in pcDNA3.1 (Invitrogen) was provided as a kind gift of Dr. Claus Pietrzik, Johannes Gutenberg University, Mainz, Germany, and served as a template for all APP695 cholesterol binding–deficient mutants. All described APP mutants were cloned using gene blocks (IDT) as mentioned above and using the restriction enzymes EcoRI and XbaI. All constructs were generated with a C-terminal FLAG tag. pIR-NT_hSREBP2-NT with a V5 tag was provided as a kind gift by Dr. Nabil Seidah, IRCM,

Montreal, Canada. All expression vectors were verified by dideoxy sequencing (McGill Génome Québec Sequencing Center).

Cell culture and transfection

HEK 293T cells were used for all experiments, cultured at a confluency of 80–90% in Dulbecco's modified Eagle's medium (DMEM) containing 4.5 g/liter glucose, 0.584 g/liter L-glutamine, and 0.11 g/liter sodium pyruvate (Wisent) and supplemented with 10% FCS (Wisent), at 37 °C, and 5% CO_2. 2×10^5 cells per well (12-well plates) were seeded 24 h prior to transient transfections. Cells were transiently transfected with 1 μg of DNA and 2 μl of polyethylenimine (PEI) per 12 wells. For co-transfections, a DNA ratio of APP to rhomboid protease of 5:1 was used. In the case of NT-SREBP2 co-transfections with RHBDL4, DNA ratios of 1:1 or 1:2 for NT-SREBP2 to RHBDL4 were used. 36 h after transfection, cells were subjected to different treatments or lysed with TNE-lysis buffer (50 mM Tris, pH 7.4, 150 mM NaCl, 2 mM EDTA, 1% Nonidet P-40, and complete protease inhibitors, Roche Applied Science) and prepared for SDS-PAGE. In all cases, 4× LDS sample buffer (with 10% β-mercaptoethanol, Invitrogen) was added to the samples for a final concentration of 1×.

Cell culture treatments

The cell culture medium was replaced 36 h after transfection with DMEM containing 10% LPDS instead of FCS and supplemented with either 5 μM simvastatin (stock in DMSO, Sigma) alone or co-treated with 0.25 mM mevalonate (stock in water, Sigma), 40 μg/ml LDL (stock in water, Millipore), or 5 or 10 μM PF-429242 (stock in DMSO, Sigma) for 24 or 48 h, respectively. Water or DMSO was used as vehicle controls. For experiments comparing the effects of FCS to LPDS, media were changed 36 h after seeding to DMEM with 10% FCS or 10% LPDS for an additional 24 h. For cells transfected with RHBDL4 mutants, treatments with 10% LPDS were started 12 h post-transfection for a duration of 24 h. Post-treatment, cells were lysed and prepared for SDS-PAGE analysis as mentioned above. All treatments were performed according to published data (30, 37, 39, 52).

Western blot analysis

Samples were separated on 4–12% bis-tris gels (Novex, NuPAGE, Invitrogen) for endogenous APP CTFs or 10–20% tris-Tricine gels for co-transfected samples. The bis-tris gels were run with MES running buffer (Invitrogen). Proteins were transferred onto nitrocellulose with transfer buffer containing 10% ethanol. The following primary antibodies were used: 22C11 (Millipore); 6E10 (Covance); mouse anti-Myc (9B11, Cell Signaling); mouse anti-β-actin (8H10D10, Cell Signaling); rabbit anti-V5 (D3H8Q, Cell Signaling); rabbit anti-FLAG (D6W5B, Cell Signaling); and Y188 (rabbit, Epitope: amino acids 750–770 of APP 770; ab32136, Abcam). HRP-coupled secondary antibodies directed against mouse or rabbit IgG were purchased from Promega. Chemiluminescence images were acquired using the ImageQuant LAS 500 or 600 system (GE Healthcare).

Pulldown with biotinylated cholesterol

A total of 2×10^6 HEK 293T cells were transfected with 10 μg of DNA and 20 μl of PEI. 36 h post-transfection, crude membrane extracts were prepared by scraping and douncing cells in PBS. Samples were split into six tubes, and membrane fractions were spun down at 10,000 rpm for 5 min. Membrane fractions were resuspended in lysis buffer (PBS + 0.3% Nonidet P-40 + 50 mM NaCl) and incubated with 20 μM alkyne cholesterol (Sigma) in 38 mM methyl-β-cyclodextrin overnight. Total cell lysates were taken as expression controls. 50 μg of protein were then subjected to a click reaction (100 μM tris(benzyltriazolylmethyl)amine, 20 μM biotin-azide, 1 mM $CuSO_4$, 1 mM tris(2-carboxyethyl)phosphine) for 1 h at room temperature. Samples were diluted with PBS, and 50 μl of neutravidin beads (ThermoFisher Scientific) were added overnight. Beads were washed twice with lysis buffer and three times with PBS. Samples were run on 4–12% bis-tris gels.

Quantitative real time PCR (RT-qPCR)

mRNA was isolated from HEK 293T cells using the Macherey and Nagel mRNA isolation kit. 2 μg of RNA were transcribed into cDNA using the high-capacity cDNA reverse transcription kit (Applied Biosystems). RT-qPCR was performed using the SsoAdvanced SYBR Green supermix (Bio-Rad) on a CFX384Touch cycler (Bio-Rad). All primers were ordered from Integrated DNA Technologies and Origene. Primers used were as follows: APP forward (CCTTCTCGTTCCTGACAAGTGC) and reverse (GGCAGCAACATGCCGTAGTCAT); GAPDH forward (GTCTCCTCTGACTTCAACAGC) and reverse (ACCACCCTGTTGCTGTAGCCAA); and β-actin forward (CACCATTGGCAATGAGCGGTTC) and reverse (AGGTCTTTGCGGATGTCCACGT). Primer efficiency for all primers was determined to be between 90 and 110%. Optimal melting temperature was determined to be 57 °C as well as a 1:80 cDNA dilution. For normalization of APP gene expression, GAPDH and β-actin were confirmed to be stable and thus were used as reference genes. RT-qPCR was analyzed using the CFX Maestro software (Bio-Rad). Data are displayed as mean expression.

Bioinformatics

RHBDL4 sequences for 72 different species were taken from Uniprot (as of September 9, 2017), and sequence homology was analyzed with the Clustal Omega Multiple Sequence Alignment tool from EMBL-EBI. Degree of conservation was determined for CRAC in transmembrane sequence 6 and CARC in transmembrane sequence 3.

Homology model for RHBDL4

The homology model of the rhomboid domain of RHBDL4 (UniProt ID Q8TEB9, from Asn-26 to Glu-215) was constructed using the intensive homology modeling of the web-based tool Phyre2, which relies on multiple template modeling (53). The templates that were selected for modeling are the crystal structures of GlpG from *Escherichia coli* (PDB code 3B45, chain A (54)) and *Haemophilus influenzae* (PDB code 2NR9, chain A (55)). This structural model was used to visualize potential intra-molecular interactions of RHBDL4

that could help interpret observations from the site-directed mutagenesis data. Our choice of the homology modeling software is based on previous observations that Phyre2 can provide a reasonable description of the core structure of the protein (within 2–4 Å root-mean-squared deviation of the native protein structure) even when the sequence identity between the target and template sequences is within 20% (56).

Data analysis and statistics

Western blotting images were quantified with ImageJ. Statistical data analysis was performed with GraphPad Prism 6, and applied tests are indicated in the figure legends.

Author contributions—S. P., J. C. Y., and L. M. M. conceptualization; S. P. formal analysis; S. P., S. J. R., A. N. B., and L. M. M. investigation; S. P. and J. C. Y. visualization; S. P., S. J. R., J. C. Y., A. N. B., and L. M. M. methodology; S. P. writing-original draft; S. J. R. validation; J. C. Y. and L. M. M. supervision; J. C. Y. and L. M. M. funding acquisition; J. C. Y., A. N. B., and L. M. M. writing-review and editing.

Acknowledgments—We thank Dr. Claus Pietrzik and Dr. Nabil Seidah for kindly providing plasmid cDNAs. We thank Meijuan Niu for valuable help with DNA cloning.

References

1. Lemberg, M. K., and Freeman, M. (2007) Functional and evolutionary implications of enhanced genomic analysis of rhomboid intramembrane proteases. *Genome Res.* **17,** 1634–1646 CrossRef Medline
2. Baker, R. P., Wijetilaka, R., and Urban, S. (2006) Two *Plasmodium* rhomboid proteases preferentially cleave different adhesins implicated in all invasive stages of malaria. *PLoS Pathog.* **2,** e113 CrossRef Medline
3. Shen, B., Buguliskis, J. S., Lee, T. D., and Sibley, L. D. (2014) Functional analysis of rhomboid proteases during *Toxoplasma* invasion. *MBio* **5,** e01795-14 Medline
4. Lemberg, M. K., and Adrain, C. (2016) Inactive rhomboid proteins: new mechanisms with implications in health and disease. *Semin. Cell Dev. Biol.* **60,** 29–37 CrossRef Medline
5. Spinazzi, M., and De Strooper, B. (2016) PARL: the mitochondrial rhomboid protease. *Semin. Cell Dev. Biol.* **60,** 19–28 CrossRef Medline
6. Civitarese, A. E., MacLean, P. S., Carling, S., Kerr-Bayles, L., McMillan, R. P., Pierce, A., Becker, T. C., Moro, C., Finlayson, J., Lefort, N., Newgard, C. B., Mandarino, L., Cefalu, W., Walder, K., Collier, G. R., *et al.* (2010) Regulation of skeletal muscle oxidative capacity and insulin signaling by the mitochondrial rhomboid protease PARL. *Cell Metab.* **11,** 412–426 CrossRef Medline
7. Shi, G., Lee, J. R., Grimes, D. A., Racacho, L., Ye, D., Yang, H., Ross, O. A., Farrer, M., McQuibban, G. A., and Bulman, D. E. (2011) Functional alteration of PARL contributes to mitochondrial dysregulation in Parkinson's disease. *Hum. Mol. Genet.* **20,** 1966–1974 CrossRef Medline
8. Walder, K., Kerr-Bayles, L., Civitarese, A., Jowett, J., Curran, J., Elliott, K., Trevaskis, J., Bishara, N., Zimmet, P., Mandarino, L., Ravussin, E., Blangero, J., Kissebah, A., and Collier, G. (2005) The mitochondrial rhomboid protease PSARL is a new candidate gene for type 2 diabetes. *Diabetologia* **48,** 459–468 CrossRef Medline
9. Paschkowsky, S., Hamzé, M., Oestereich, F., and Munter, L. M. (2016) Alternative processing of the amyloid precursor protein family by rhomboid protease RHBDL4. *J. Biol. Chem.* **291,** 21903–21912 CrossRef Medline
10. Düsterhoft, S., Künzel, U., and Freeman, M. (2017) Rhomboid proteases in human disease: mechanisms and future prospects. *Biochim. Biophys. Acta* **1864,** 2200–2209 CrossRef Medline
11. Paschkowsky, S., Oestereich, F., and Munter, L. M. (2018) Embedded in the membrane: how lipids confer activity and specificity to intramembrane proteases. *J. Membr. Biol.* **251,** 369–378 Medline
12. Urban, S., and Wolfe, M. S. (2005) Reconstitution of intramembrane proteolysis *in vitro* reveals that pure rhomboid is sufficient for catalysis and specificity. *Proc. Natl. Acad. Sci. U.S.A.* **102,** 1883–1888 CrossRef Medline
13. Moin, S. M., and Urban, S. (2012) Membrane immersion allows rhomboid proteases to achieve specificity by reading transmembrane segment dynamics. *Elife* **1,** e00173 CrossRef Medline
14. Urban, S., and Moin, S. M. (2014) A subset of membrane-altering agents and γ-secretase modulators provoke nonsubstrate cleavage by rhomboid proteases. *Cell Rep.* **8,** 1241–1247 CrossRef Medline
15. Fleig, L., Bergbold, N., Sahasrabudhe, P., Geiger, B., Kaltak, L., and Lemberg, M. K. (2012) Ubiquitin-dependent intramembrane rhomboid protease promotes ERAD of membrane proteins. *Mol. Cell* **47,** 558–569 CrossRef Medline
16. Wunderle, L., Knopf, J. D., Kühnle, N., Morlé, A., Hehn, B., Adrain, C., Strisovsky, K., Freeman, M., and Lemberg, M. K. (2016) Rhomboid intramembrane protease RHBDL4 triggers ER-export and non-canonical secretion of membrane-anchored TGFα. *Sci. Rep.* **6,** 27342 CrossRef Medline
17. van Meer, G., Voelker, D. R., and Feigenson, G. W. (2008) Membrane lipids: where they are and how they behave. *Nat. Rev. Mol. Cell Biol.* **9,** 112–124 CrossRef Medline
18. Motamed, M., Zhang, Y., Wang, M. L., Seemann, J., Kwon, H. J., Goldstein, J. L., and Brown, M. S. (2011) Identification of luminal Loop 1 of Scap protein as the sterol sensor that maintains cholesterol homeostasis. *J. Biol. Chem.* **286,** 18002–18012 CrossRef Medline
19. Brown, M. S., Ye, J., Rawson, R. B., and Goldstein, J. L. (2000) Regulated intramembrane proteolysis: a control mechanism conserved from bacteria to humans. *Cell* **100,** 391–398 CrossRef Medline
20. Barrett, P. J., Song, Y., Van Horn, W. D., Hustedt, E. J., Schafer, J. M., Hadziselimovic, A., Beel, A. J., and Sanders, C. R. (2012) The amyloid precursor protein has a flexible transmembrane domain and binds cholesterol. *Science* **336,** 1168–1171 CrossRef Medline
21. Beel, A. J., Mobley, C. K., Kim, H. J., Tian, F., Hadziselimovic, A., Jap, B., Prestegard, J. H., and Sanders, C. R. (2008) Structural studies of the transmembrane C-terminal domain of the amyloid precursor protein (APP): does APP function as a cholesterol sensor? *Biochemistry* **47,** 9428–9446 CrossRef Medline
22. Munter, L. M., Voigt, P., Harmeier, A., Kaden, D., Gottschalk, K. E., Weise, C., Pipkorn, R., Schaefer, M., Langosch, D., and Multhaup, G. (2007) GxxxG motifs within the amyloid precursor protein transmembrane sequence are critical for the etiology of Aβ42. *EMBO J.* **26,** 1702–1712 CrossRef Medline
23. Pierrot, N., Tyteca, D., D'Auria, L., Dewachter, I., Gailly, P., Hendrickx, A., Tasiaux, B., Haylani, L. E., Muls, N., N'Kuli, F., Laquerrière, A., Demoulin, J. B., Campion, D., Brion, J. P., Courtoy, P. J., *et al.* (2013) Amyloid precursor protein controls cholesterol turnover needed for neuronal activity. *EMBO Mol. Med.* **5,** 608–625 CrossRef Medline
24. Miller, L. J., and Chacko, R. (2004) The role of cholesterol and statins in Alzheimer's disease. *Ann. Pharmacother.* **38,** 91–98 CrossRef Medline
25. Puglielli, L., Tanzi, R. E., and Kovacs, D. M. (2003) Alzheimer's disease: the cholesterol connection. *Nat. Neurosci.* **6,** 345–351 CrossRef Medline
26. Wolozin, B. (2001) A fluid connection: cholesterol and Aβ. *Proc. Natl. Acad. Sci. U.S.A.* **98,** 5371–5373 CrossRef Medline
27. Hwang, J., Ribbens, D., Raychaudhuri, S., Cairns, L., Gu, H., Frost, A., Urban, S., and Espenshade, P. J. (2016) A Golgi rhomboid protease Rbd2 recruits Cdc48 to cleave yeast SREBP. *EMBO J.* **35,** 2332–2349 CrossRef Medline
28. Kim, J., Ha, H. J., Kim, S., Choi, A. R., Lee, S. J., Hoe, K. L., and Kim, D. U. (2015) Identification of Rbd2 as a candidate protease for sterol regulatory element binding protein (SREBP) cleavage in fission yeast. *Biochem. Biophys. Res. Commun.* **468,** 606–610 CrossRef Medline
29. Goldstein, J. L., and Brown, M. S. (1990) Regulation of the mevalonate pathway. *Nature* **343,** 425–430 CrossRef Medline
30. Ferreri, K., Talavera, F., and Menon, K. M. (1992) Increased cellular cholesterol upregulates high density lipoprotein binding to rat luteal cells. *Endocrinology* **131,** 2059–2064 CrossRef Medline

31. Goldstein, J. L., and Brown, M. S. (2015) A century of cholesterol and coronaries: from plaques to genes to statins. *Cell* **161,** 161–172 CrossRef Medline
32. Fassbender, K., Simons, M., Bergmann, C., Stroick, M., Lutjohann, D., Keller, P., Runz, H., Kuhl, S., Bertsch, T., von Bergmann, K., Hennerici, M., Beyreuther, K., and Hartmann, T. (2001) Simvastatin strongly reduces levels of Alzheimer's disease β-amyloid peptides Aβ42 and Aβ40 *in vitro* and *in vivo*. *Proc. Natl. Acad. Sci. U.S.A.* **98,** 5856–5861 CrossRef Medline
33. Frears, E. R., Stephens, D. J., Walters, C. E., Davies, H., and Austen, B. M. (1999) The role of cholesterol in the biosynthesis of β-amyloid. *Neuroreport* **10,** 1699–1705 CrossRef Medline
34. Kojro, E., Füger, P., Prinzen, C., Kanarek, A. M., Rat, D., Endres, K., Fahrenholz, F., and Postina, R. (2010) Statins and the squalene synthase inhibitor zaragozic acid stimulate the non-amyloidogenic pathway of amyloid-β protein precursor processing by suppression of cholesterol synthesis. *J. Alzheimers Dis.* **20,** 1215–1231 CrossRef Medline
35. Kojro, E., Gimpl, G., Lammich, S., Marz, W., and Fahrenholz, F. (2001) Low cholesterol stimulates the nonamyloidogenic pathway by its effect on the α-secretase ADAM 10. *Proc. Natl. Acad. Sci. U.S.A.* **98,** 5815–5820 CrossRef Medline
36. Sidera, C., Parsons, R., and Austen, B. (2005) The regulation of β-secretase by cholesterol and statins in Alzheimer's disease. *J. Neurol. Sci.* **229,** 269–273 Medline
37. Cole, S. L., Grudzien, A., Manhart, I. O., Kelly, B. L., Oakley, H., and Vassar, R. (2005) Statins cause intracellular accumulation of amyloid precursor protein, β-secretase-cleaved fragments, and amyloid β-peptide via an isoprenoid-dependent mechanism. *J. Biol. Chem.* **280,** 18755–18770 CrossRef Medline
38. Sakai, J., Rawson, R. B., Espenshade, P. J., Cheng, D., Seegmiller, A. C., Goldstein, J. L., and Brown, M. S. (1998) Molecular identification of the sterol-regulated luminal protease that cleaves SREBPs and controls lipid composition of animal cells. *Mol. Cell* **2,** 505–514 CrossRef Medline
39. Hawkins, J. L., Robbins, M. D., Warren, L. C., Xia, D., Petras, S. F., Valentine, J. J., Varghese, A. H., Wang, I. K., Subashi, T. A., Shelly, L. D., Hay, B. A., Landschulz, K. T., Geoghegan, K. F., and Harwood, H. J., Jr. (2008) Pharmacologic inhibition of site 1 protease activity inhibits sterol regulatory element-binding protein processing and reduces lipogenic enzyme gene expression and lipid synthesis in cultured cells and experimental animals. *J. Pharmacol. Exp. Ther.* **326,** 801–808 CrossRef Medline
40. Janowski, B. A. (2002) The hypocholesterolemic agent LY295427 up-regulates INSIG-1, identifying the INSIG-1 protein as a mediator of cholesterol homeostasis through SREBP. *Proc. Natl. Acad. Sci. U.S.A.* **99,** 12675–12680 CrossRef Medline
41. Goldstein, J. L., Basu, S. K., and Brown, M. S. (1983) Receptor-mediated endocytosis of low-density lipoprotein in cultured cells. *Methods Enzymol.* **98,** 241–260 CrossRef Medline
42. Amemiya-Kudo, M., Shimano, H., Hasty, A. H., Yahagi, N., Yoshikawa, T., Matsuzaka, T., Okazaki, H., Tamura, Y., Iizuka, Y., Ohashi, K., Osuga, J., Harada, K., Gotoda, T., Sato, R., Kimura, S., *et al.* (2002) Transcriptional activities of nuclear SREBP-1a, -1c, and -2 to different target promoters of lipogenic and cholesterogenic genes. *J. Lipid Res.* **43,** 1220–1235 Medline
43. Fantini, J., Di Scala, C., Evans, L. S., Williamson, P. T., and Barrantes, F. J. (2016) A mirror code for protein-cholesterol interactions in the two leaflets of biological membranes. *Sci. Rep.* **6,** 21907 CrossRef Medline
44. Baier, C. J., Fantini, J., and Barrantes, F. J. (2011) Disclosure of cholesterol recognition motifs in transmembrane domains of the human nicotinic acetylcholine receptor. *Sci. Rep.* **1,** 69 CrossRef Medline
45. Li, H., and Papadopoulos, V. (1998) Peripheral-type benzodiazepine receptor function in cholesterol transport. Identification of a putative cholesterol recognition/interaction amino acid sequence and consensus pattern. *Endocrinology* **139,** 4991–4997 CrossRef Medline
46. Gál, Z., Hegedüs, C., Szakács, G., Váradi, A., Sarkadi, B., and Özvegy-Laczka, C. (2015) Mutations of the central tyrosines of putative cholesterol recognition amino acid consensus (CRAC) sequences modify folding, activity, and sterol-sensing of the human ABCG2 multidrug transporter. *Biochim. Biophys. Acta* **1848,** 477–487 CrossRef Medline
47. Bondar, A. N., del Val, C., and White, S. H. (2009) Rhomboid protease dynamics and lipid interactions. *Structure* **17,** 395–405 CrossRef Medline
48. Arutyunova, E., Strisovsky, K., and Lemieux, M. J. (2017) Activity assays for rhomboid proteases. *Methods Enzymol.* **584,** 395–437 CrossRef Medline
49. Das, A., Brown, M. S., Anderson, D. D., Goldstein, J. L., and Radhakrishnan, A. (2014) Three pools of plasma membrane cholesterol and their relation to cholesterol homeostasis. *Elife* **3,** e02882 CrossRef Medline
50. Willem, M., Tahirovic, S., Busche, M. A., Ovsepian, S. V., Chafai, M., Kootar, S., Hornburg, D., Evans, L. D., Moore, S., Daria, A., Hampel, H., Müller, V., Giudici, C., Nuscher, B., Wenninger-Weinzierl, A., *et al.* (2015) η-Secretase processing of APP inhibits neuronal activity in the hippocampus. *Nature* **526,** 443–447 CrossRef Medline
51. Wang, H., Sang, N., Zhang, C., Raghupathi, R., Tanzi, R. E., and Saunders, A. (2015) Cathepsin L mediates the degradation of novel APP C-terminal fragments. *Biochemistry* **54,** 2806–2816 CrossRef Medline
52. Gbelcová, H., Svéda, M., Laubertová, L., Varga, I., Vítek, L., Kolář, M., Strnad, H., Zelenka, J., Böhmer, D., and Ruml, T. (2013) The effect of simvastatin on lipid droplets accumulation in human embryonic kidney cells and pancreatic cancer cells. *Lipids Health Dis.* **12,** 126 CrossRef Medline
53. Kelley, L. A., Mezulis, S., Yates, C. M., Wass, M. N., and Sternberg, M. J. (2015) The Phyre2 web portal for protein modeling, prediction and analysis. *Nat. Protoc.* **10,** 845–858 CrossRef Medline
54. Wang, Y., Maegawa, S., Akiyama, Y., and Ha, Y. (2007) The role of L1 loop in the mechanism of rhomboid intramembrane protease GlpG. *J. Mol. Biol.* **374,** 1104–1113 CrossRef Medline
55. Lemieux, M. J., Fischer, S. J., Cherney, M. M., Bateman, K. S., and James, M. N. (2007) The crystal structure of the rhomboid peptidase from *Haemophilus influenzae* provides insight into intramembrane proteolysis. *Proc. Natl. Acad. Sci. U.S.A.* **104,** 750–754 CrossRef Medline
56. Kelley, L. A., and Sternberg, M. J. (2009) Protein structure prediction on the Web: a case study using the Phyre server. *Nat. Protoc.* **4,** 363–371 CrossRef Medline
57. Humphrey, W., Dalke, A., and Schulten, K. (1996) VMD: visual molecular dynamics. *J. Mol. Graph.* **14,** 33–38, 27–38 CrossRef